J Biol Phys (2006) 32: 231–243
DOI 10.1007/s10867-006-9014-z

RESEARCH PAPER

Optimal Length Transportation Hypothesis to Model Proteasome Product Size Distribution

Alexey Zaikin · Juergen Kurths

Received: 15 January 2006 / Accepted: 10 February 2006 /
Published online: 26 October 2006

Abstract This paper discusses translocation features of the 20S proteasome in order to explain typical proteasome length distributions. We assume that the protein transport depends significantly on the fragment length with some optimal length which is transported most efficiently. By means of a simple one-channel model, we show that this hypothesis can explain both the one- and the three-peak length distributions found in experiments. A possible mechanism of such translocation is provided by so-called fluctuation-driven transport.

Key words proteasome · protein translocation · stochastic process · ratchets

1 Introduction

Proteasomes are multicatalytic cellular protease complexes that degrade intracellular proteins into smaller peptides. They are present in all eukaryotic cells, archaea, and certain bacteria [1–3]. In experiments [4] about 5×10^5 proteasomes have been found in the nucleus and the cytoplasm of a single eukaryotic cell. Estimating the total cell number in a human body to be 6×10^{13} and the degradation time of an average 400 amino acid (aa) long protein as 3.5 min [5] we come to the conclusion that approximately 8.5×10^{18} proteins must be destroyed in our body by proteasomes each minute. Proteasomes are absolutely essential for cellular homeostasis, and the removal of proteasome genes in eukaryotes is lethal [6]. Many roles in the cell's metabolism are played by proteasomes: they destroy abnormal and misfolded proteins tagged with ubiquitin and are an essential component of the ATP-Ubiquitin-dependent pathway for protein degradation [7, 8]. Proteasomes play an important role in the immune system by generating antigenic peptides of 8–12 residues to be presented by the MHC class I molecules and, hence, are the main

A. Zaikin (✉) · J. Kurths
Institute of Physics, University of Potsdam, D-14415 Potsdam, Germany
e-mail: a.zaikin@berlin.de

supplier of peptides for their recognition by killer T-cells [2, 9–13]. As a part of the Ubiquitin system, proteasomes are involved in the regulation of the cell cycle and the cell stress response. Recently, proteasome inhibition has been suggested as a promising new target for cancer treatment [14–16]. Proteasome function has also been linked directly to the pathophysiology of malignancies, neurodegenerative disorders, type I diabetes, cachexia [17, 18] and to ageing [19].

Proteasomes have been found in the form of different, although similar molecular complexes that consist of a central part, the 20S proteasome, and regulating caps, the 19S [1] and PA28 particles [20, 21]. The most important 26S complex, which degrades ubiquitinated proteins, contains in addition to the 20S proteasome a 19S regulatory complex composed of multiple ATPases and components necessary for binding protein substrates [1]. The 20S proteasome is a barrel-shaped structure composed of four stacked rings of 28 subunits [1, 22]. The active cleavage sites are located within the central chamber of the 20S proteasome, into which protein substrates must enter through narrow openings of outer rings. The 20S proteasome degrades proteins by a highly processive mechanism [23], making many cleavages of the protein and digesting it into small products. This is important for the intracellular proteolytic system because the release of large protein fragments could interfere with the cell function and regulation [5]. Proteasomes can be found in their usual form as a constitutive proteasome, or as an immunoproteasome with modified cleavage centers [2, 10].

Due to its significance in cellular metabolism, the simulation of proteasome function is the central task in the building of a virtual immune system [24]. On the long road from the initial idea to the launch of a new drug at the pharmacy the simulation and prediction of proteasome function seem to be possible now only in the early stages of drug design, i.e., for *in vitro* experiments. Such experiments study the digestion of different substrates by the proteasome and the temporal dynamics of the fragment concentration over the course of time by mixing purified proteasomes with different substrates. The experimental results are analyzed, for example, by mass spectroscopy methods and provide us with information about the substrate cleavage pattern and the quantity of different fragments cut from the initial substrate. Even in these first stages of drug design, however, the simulation of proteasome could significantly reduce experimental costs through identification and prediction of proper parameter ranges.

One of the most important experimental results that describes proteasome function is a length distribution of the fragments obtained *in vitro* experiments by the analysis of generated cleavage products. For long substrates, it was found that this dependence typically is nonmonotonic and has a single peak around the length of 7–12 amino acids (aa) for practically all types of proteasome [5, 25–27]. It is important to note that this peptide length is the most critical length for normal functioning of the immune system. The proteasome products can also be a little bit longer because they can be cut further by proteases. The mechanism behind such a length distribution is not completely clear. It was widely believed that the proteasome degrades proteins according to a ‘molecular ruler’ to yield products of rather uniform size, as first proposed by [28]. It was suggested that peptides of seven to nine residues were generated as a result of coordinated cleavages by neighboring active sites. However, evidence for the molecular ruler is quite limited because the maximum in the length distribution is fairly broad and not pronounced as a sharp

peak [5]. It is also interesting to note that, in some experiments, three-peak length distributions have been found [29].

To model the proteasome mechanism one should adequately describe three essential processes involved in proteasome function: selection of cleavage sites, kinetics of generated fragments, and peptide translocation inside the proteasome. Three algorithms are available for the prediction of cleavage sites, PAProC [30], Netchop [31], and ProteaSMM [32]. Several theoretical models for the kinetics of proteasome degradation have been published. Some of the models describe the degradation of short peptides with qualitatively different kinetics [33–35] or small number of cleavage positions [36]. The theoretical model [36, 37] for the degradation of long substrates is applied to specific proteins with predefined cleavage sites and is fitted to experimental data describing the fragment quantity after proteasomal degradation.

Much less attention has been paid in the literature to the description of peptide translocation inside the proteasome chamber. To fill this gap the present paper addresses solely protein translocation in order to show that differences in length-dependent velocity rates can be of crucial importance for length distribution. With this purpose, we suggest a simple one-channel proteasome model that describes the translocation and the cleavage of a substrate, as well as of the generated fragments. Next, we perform simulations with two typical qualitatively different translocation rate functions and show that the nonmonotonic function can result in one- or three-peak length distributions. Finally, we discuss a possible mechanism behind such translocation rates, and consider the influence of sequence specificity on the results of our model.

2 Model

Our model assumes that the proteasome has one channel only, and two cleavage centers, i.e., a symmetric structure as seen experimentally. The two cleavage centers represent the projection on the translocation route of the cleavage centers of the two internal rings, which in reality can have up to six cleavage centers which are distributed in the 3D structure. The substrate which enters this channel can be cleaved or translocated together with the generated fragments until they leave the channel (see Figure 1). The translocation and cleavage are modelled by the Gillespie algorithm according to the translocation and cleavage rates [38]. According to this

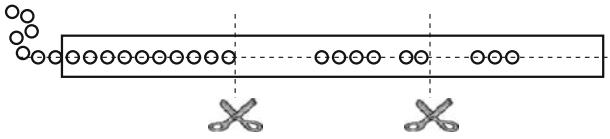

Figure 1 Model of the proteasome with two cleavage centers. A protein with unspecified sequence (denoted as '0-0-0-0') enters the single proteasome channel from the *left*. It can be cleaved at any point by cleavage sites denoted by scissors. The cleavage rate can depend on the position. The cleaved fragments move with different velocities depending on their length. After a waiting time, computed by means of the Gillespie algorithm, either cleavage or translocation may occur.

algorithm we can stochastically model the system where several events can happen with different probabilities. Suppose that at some moment of time we have a set of N probable events with rates R_i, where the ith event has the rate R_i and $i = 1..N$. Then, by generating two uniformly distributed random numbers RN_1 and RN_2, we estimate the time T after which the next event is likely to occur as

$$T = -\frac{\log(RN_1)}{\sum_i^N R_i}. \tag{1}$$

The actual event k that occurs after this time can be determined by:

$$\sum_i^k R_i < \sum_i^N R_i RN_2 \leq \sum_i^{k+1} R_i. \tag{2}$$

The peptide or its part inside the proteasome can either be shifted by one amino acid or it can be cleaved if it is located near the cleavage center. In this version of the model, overtaking of fragments is forbidden, just as the peptide cannot be translocated into a position already occupied by another fragment. Inside the proteasome, the translocation rates of the substrate or fragments depend only on their lengths and are described by the translocation rate function $R_t(l)$, where l is the length of the substrate or fragment part which is inside the proteasome. Hence if the initial substrate enters the proteasome, this length will be increased. According to this function fragments of different length can have different translocation rates. The probability of cleavage is described by the function $R_c(p)$, where p is the position in the substrate sequence. For generated fragments the cleavage rates remain the same as they were in the initial substrate for the corresponding positions. We assume that the substrate is degraded by a processive mechanism, i.e., the protein cannot move back and cannot leave the proteasome from the other side until completely processed (for experimental argument see [23]). When the protein is degraded, its fragment lengths are counted in the length distribution. To obtain reliable statistics, the length distribution is averaged over a large number of proteins N. This also corresponds to the usual experimental set up. The standard parameters that are used in the simulations are given in Table I together with their default values.

3 Results

First, let us fix all the cleavage rates $R_c(p)$ to a constant and show that different translocation rates can result in qualitatively different forms of length distribution.

Table I Parameter values of the model

Parameter	Description	Dimension	Default value
l	Fragment length	Amino acids	-
L_p	Protein length	Amino acids	300
L	Proteasome length	Amino acids	80
D	Distance between a cleavage center and the proteasome end	Amino acids	15
N	Number of degraded proteins	-	10^4

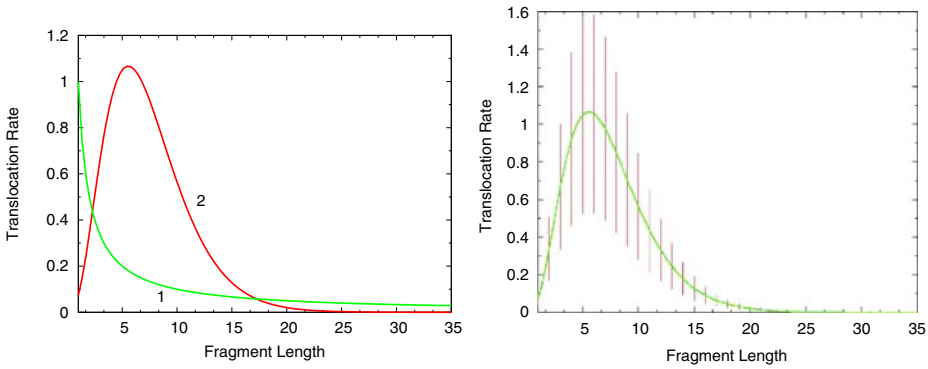

Figure 2 *Left*: two qualitatively different forms of translocation rates used in the model (see Sec. 2), a monotonically decreasing function $R1(l)$ (*curve 1*) and a nonmonotonous function $R2(l)$ (*curve 2*) with one maximum at the most optimal translocation length. For exact expressions see the text. *Right*: translocation rate function $R2(l)$ and the intervals of its random variation (*vertical bars*).

To check different translocation rate functions, we have used a decreasing function $R_t(l) = R1(l) = 1/l$ and a nonmonotonic function $R_t(l) = R2(l) = (0.5l)^3 e^{-\alpha l}$ with $\alpha = 0.54$ (Figure 2, left). If the cleavage rates are relatively high ($R_c(p) = 0.01$), the difference in the length distribution will not be very pronounced because the probability of cleavage will dominate over the probability of translocation and, as a result, short fragments will dominate in the length distribution. Comparing Figure 3, left and right, we see that for both translocation rate functions the length distribution is a monotonically decreasing function.

The situation changes qualitatively if cleavage rates are not so high, e.g., $R_c(p) = 0.001$ (see Figure 4). For a monotonically decreasing function, the length distribution is also monotonically decreasing (left). However, for the translocation rate function with the optimal length for transportation, one can clearly see a peak in the length distribution (right). Hence we have shown that translocation rate dependences can be of crucial importance for length distributions. If this function is nonmonotonic and has a clearly defined optimal transportation length, this can result in a single-peak

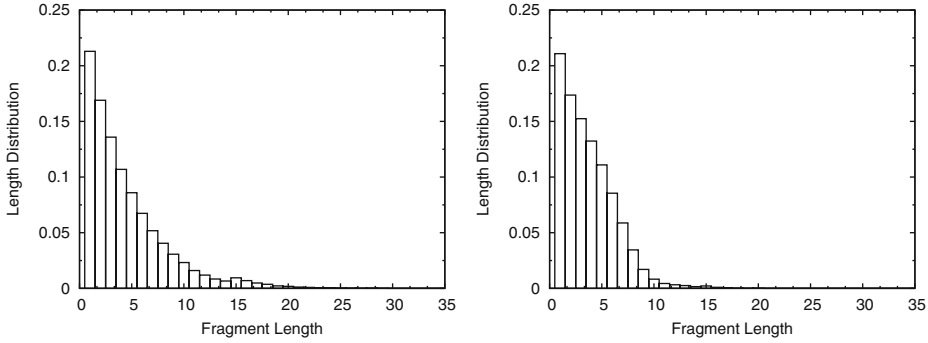

Figure 3 Length distribution for $R1(l)$ and $R_c(p) = 0.01$ (*left*) and for $R2(l)$ and $R_c(p) = 0.01$ (*right*).

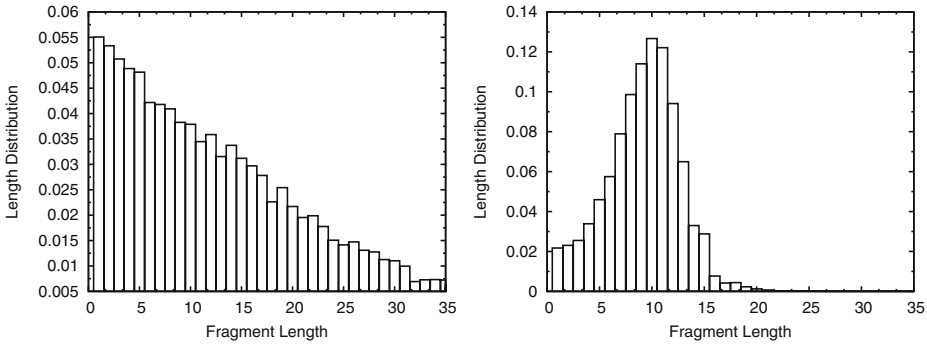

Figure 4 Length distribution for $R1(l)$, $R_c(p) = 0.001$ (*left*) and for $R2(l)$, $R_c(p) = 0.001$ (*right*). It is clearly seen that nonmonotonic translocation rate can result in one-peak distributions.

length distribution as observed in numerous experiments [5, 25–27]. Since the length corresponding to this peak is the most important length for the immune system, we conclude that translocation properties of the protein should be taken into account in the creation of the virtual proteasome system. Interestingly, tuning the parameters, namely setting $R_t(l) = R2(l), \alpha = 0.47$, and $D = 20$, one can also obtain a three-peak length distribution (Figure 5, left) as found in experiments by degradation of casein with size-exclusion chromatography [29].

We have presented here an optimal length transportation hypothesis and discussed how nonmonotonic translocation rate functions can play an important role in the production of the nonmonotonic length distribution found in many experiments. A question naturally arises: what is the mechanism behind such translocation rates? Let us discuss one of the possible translocation mechanisms behind nonmonotonic translocation rate functions. In [39] we have assumed that the proteasome has a fluctuationally-driven transport mechanism and shown that such a mechanism generally results in a nonmonotonic translocation rate. Since the proteasome has a symmetric structure, three ingredients are required for fluctuationally-driven translocation: an anisotropy of the proteasome–protein interaction potential, thermal noise

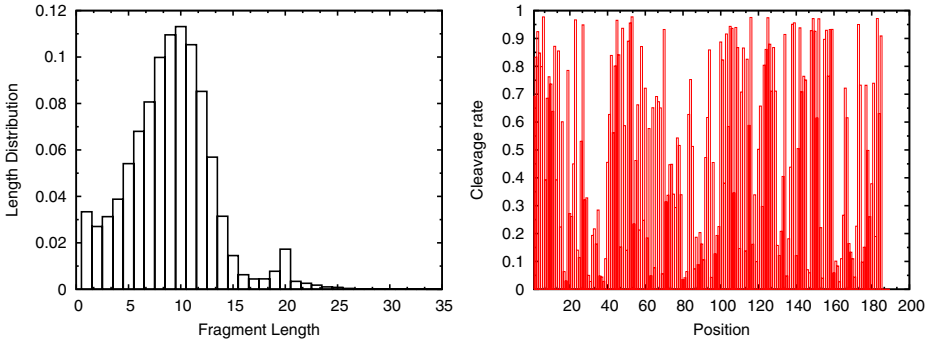

Figure 5 *Left*: three-peak length distribution for $R2(l)$, $R_c(p) = 0.001$, $\alpha = 0.47$, $D = 20$. *Right*: Casein cleavage strength pattern computed with Netchop.

in the interaction centers, and an energy input. Under the assumption that the protein potential is asymmetric and periodic, and that the energy input is modeled with a periodic force or colored noise, one can even obtain nonmonotonic translocation rates analytically [39]. Here we review these results and show that for different forms of the proteasome–protein interaction potential one gets nonmonotonic translocation rates.

We assume that after the protein has entered the proteasome, the protein–proteasome interaction is characterized by a spatially periodic asymmetric potential $U(x)$ with the period P equal to the distance between amino acids in the protein. In reality there is a basic periodicity, namely the periodicity of the protein (or peptide) backbone, that is superposed by a non-periodic (in our sense irregular) part that is attributed to the amino-acid-specific residues. Below we consider also the influence of the nonperiodic constituent. The spatial asymmetry results from breaking the symmetry by entering the proteasome from one end as well as from the $C-N$ asymmetry of the protein (or peptide) backbone. On the left side of Figure 6, we

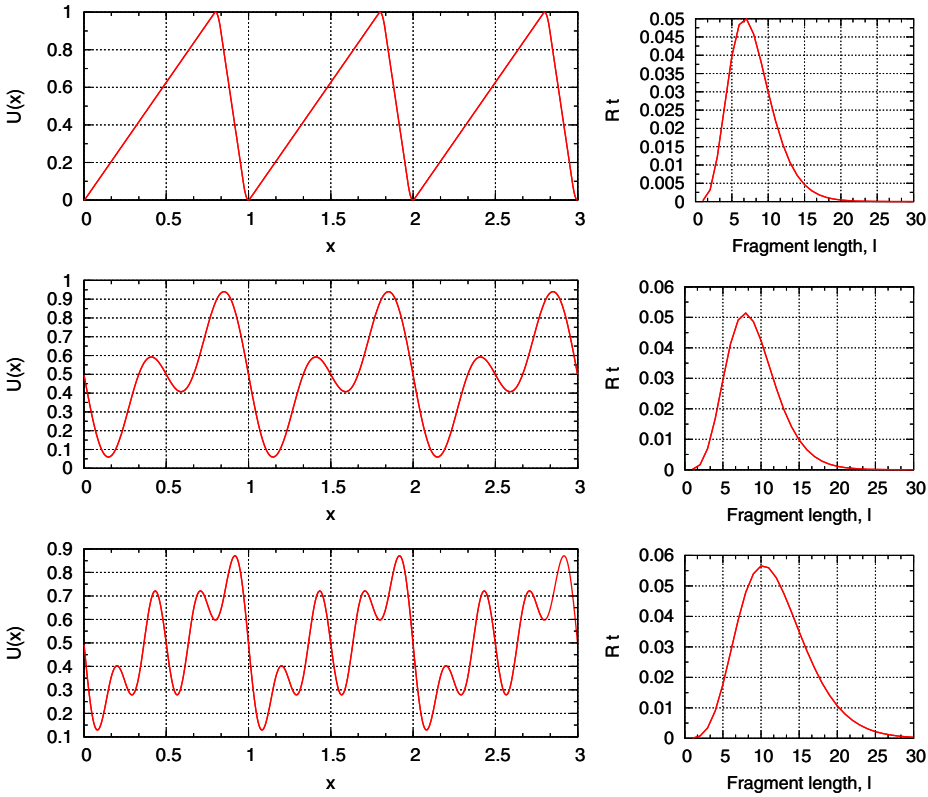

Figure 6 *Left*: different examples of asymmetric periodic potential $U(x)$ with the period $P = 1$. Only three periods are shown. From *top* to *bottom*: $U(x)$ is a saw-tooth function with smoothed angles (for details see [40]; $U(x) = -(\sin(2\pi x/P) + \sin(4\pi x/P))/4 + 0.5$; $U(x) = -(\sin(2\pi x/P) + \sin(4\pi x/P) + \sin(8\pi x/P))/6 + 0.5$. *Right*: the corresponding dependences of the velocity rate R_t on the peptide length l expressed in amino acids and $A = 1.15$.

have plotted several examples of such asymmetric periodic potentials. The detailed form of the asymmetric periodic interaction potential is of less importance for this qualitative study.

The proteasome acts upon the protein by a certain number of equidistant interaction centers. The dynamics of the protein inside the proteasome is, hence, governed by l interaction centers, where l is the number of protein elements (amino acids or multiples of them). The following forces are of significance: potential force (protein–proteasome interaction) $-l\partial U(x)/\partial x$, fluctuations with collective $lF(t)$ and individual components $f_1(t) + ... + f_l(t)$, and protein friction forces $l\beta\dot{x}$ [41], where x is the coordinate of the protein with respect to the proteasome and β is the coefficient of friction. Due to the small size of all protein particles, moving in the liquid cytosol, the motion occurs in the overdamped realm [42]. Hence, we neglect inertial forces. Note that transport is possible only in the case of nonequilibrium fluctuations. In the simplified case, when fluctuations can be represented by a sum of a collective periodic force and individual force for every protein residue resulting from thermal noise, the model is analytically tractable, predicting the velocity dependence on the peptide size. Normalizing all forces by friction and taking $\beta = 1$, the translocation of a protein in the proteasome is governed then by

$$\frac{\partial x}{\partial t} = -\frac{\partial U(x)}{\partial x} + F(t) + \frac{1}{l}(f_1(t) + ... + f_l(t)). \tag{3}$$

Analytical results are possible if we assume collective oscillations of the peptide elements, e.g., $F(t) = A\cos(\omega t)$, where A and ω stand for the amplitude and frequency of this oscillation. Additionally, each interaction center undergoes local thermal fluctuations, represented by mutually uncorrelated white noise of intensity σ^2: $f_i(t) = \xi_i(t)$, where $\langle \xi_i(t)\xi_j(t')\rangle = \sigma^2\delta(t-t')\delta_{ij}$. In this case the stochastic term in Eq. (3) is white noise of intensity σ^2/l. The Fokker–Planck equation for the peptide coordinate probability distribution $w(x,t)$ associated with Eq. (3) is

$$\frac{\partial w}{\partial t} = -\frac{\partial}{\partial x}\left[\left(F(t) - \frac{\partial U}{\partial x}\right)w(x,t)\right] + \frac{\sigma^2}{2l}\frac{\partial^2 w(x,t)}{\partial x^2}, \tag{4}$$

which may be solved in the quasi-stationary adiabatic approximation $\partial w/\partial t = 0$ [43]. We obtain

$$\frac{\sigma^2}{2l}\frac{\partial w(x,F)}{\partial x} - \left(F - \frac{\partial U}{\partial x}\right)w(x,F) = -G(F), \tag{5}$$

where $G(F)$ is the probability flux. For any periodic potential $U(x)$ the quasi-stationary solution of Eq. (5) is

$$w(x,t) = \left[C(F) - \frac{2G(F)}{\sigma^2/l}\int_0^x \exp\left(\frac{U(x') - Fx'}{\sigma^2/2l}\right)\mathrm{d}x'\right]\exp\left(-\frac{U(x) - Fx}{\sigma^2/2l}\right), \tag{6}$$

where $C(F(t))$ and $G(F(t))$ are unknown functions of t. Using the periodicity condition $w(0,t) = w(P,t)$ and the normalization of $w(x,t)$, we get $G(F)$. If the amplitude A meets the condition $LA \ll \sigma^2/l$, one can expand $G(F)$ and obtain

$$G(F) \approx G_{01}F + G_{02}F^2 \tag{7}$$

with the expansion coefficients $G_{01} = P/(I_{10}I_{20})$,

$$G_{02} = G_{01}\left(\frac{I_{11}}{I_{10}} - \frac{I_{21}}{I_{20}} - \frac{lP}{\sigma^2}\left(1 - \frac{2I_{30}}{I_{10}I_{20}}\right)\right), \quad I_{10} = \int_0^P e^{U'(x)}\,\mathrm{d}x, \tag{8}$$

$$I_{20} = \int_0^P e^{(-U'(x))}\,\mathrm{d}x, \quad I_{11} = \frac{2l}{\sigma^2}\int_0^P x e^{U'(x)}\,\mathrm{d}x, \;\; U'(x) = \frac{2lU(x)}{\sigma^2}. \tag{9}$$

$$I_{21} = \frac{2l}{\sigma^2}\int_0^P x e^{(-U'(x))}\,\mathrm{d}x \;\; I_{30} = \int_0^P \int_0^x e^{(U'(x')-U'(x))}\,\mathrm{d}x'\,\mathrm{d}x. \tag{10}$$

Substituting Eq. (7) into $\overline{\langle \dot{x} \rangle} = \int_0^P \overline{G(x,t)}\,\mathrm{d}x$, where $\overline{(\cdot)}$ denotes time averaging, we obtain the average protein transport velocity or the translocation, as a function of the noise intensity σ^2 and the peptide size l

$$R_\mathrm{t} \approx \overline{\langle \dot{x} \rangle} \approx \frac{P^2A^2}{2I_{10}I_{20}}\left[\frac{I_{11}}{I_{10}} - \frac{I_{21}}{I_{20}} - \frac{lP}{\sigma^2}\left(1 - \frac{2I_{30}}{I_{10}I_{20}}\right)\right]. \tag{11}$$

The dependences of the translocation rate on the peptide length, computed using Eq. (11), are shown in Figure 6 (right) for different interaction potentials shown in the same figure. These results show that very different forms of the interaction potential, if this potential fullfils the conditions of fluctuationally-driven transport, result in the nonmonotonic translocation rate functions.

Proteins and especially unfolded synthetic peptides have indeed a periodic constituent in the potential due to a peptide bond. However this periodicity can be hidden by an unperiodic, sequence-specific potential. In this case the real translocation rates for different fragments vary around the function computed for a non-sequence-specific case. Let us analyze how much this variation can change the length distribution. For this we perform simulations with all parameters as in Figure 4 (right), but at all simulation steps we change the translocation rate randomly up to 50% of its initial value determined by the function $R2(l)$ (see Figure 2, right). This means that at any step i the translocation rate for the fragment of the length l_i is equal to $R2(l_i)(1 + R_i)$ where R_i are random numbers uniformly distributed in the interval $[-0.5 : 0.5]$. Surprisingly, we have found that in this case the length distribution is exactly the same as in Figure 4 (right). Hence, despite the real nonperiodicity of the potential, the nonperiodic constituent is not so important for the length distribution as the periodic one, which defines the nonmonotonic rate dependence. Certainly, this is true for rather long proteins ($L_\mathrm{p} > 150$) and large statistics $N > 10^4$.

4 Discussion

We have assumed that translocation rates have nonmonotonic distributions. This may result from fluctuationally-driven transport of the protein inside the proteasome. However, it is an open question where the energy input that supplies the nonequilibrium protein translocation comes from. Here it is important to note that a translocation in the 20S proteasome can be ATP-independent. Hence, ATP molecules cannot be the only energy source if we assume active transport and not

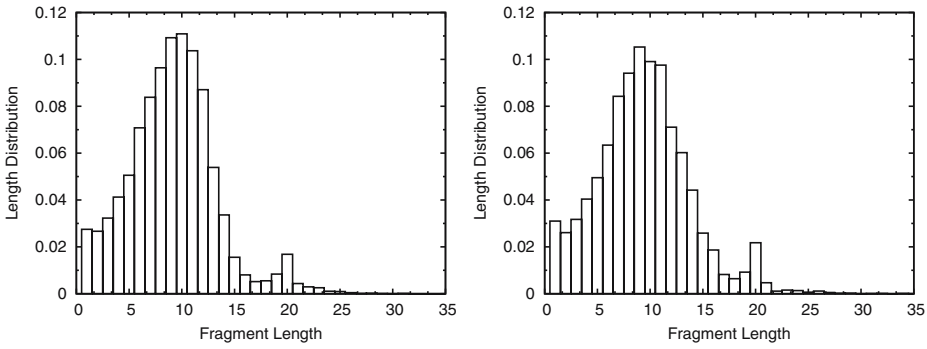

Figure 7 Length distribution as a result of casein degradation, with non-sequence-specific cleavage rates (*left*) and with the cleavage pattern computed with the Netchop algorithm (*right*).

diffusion to be the driving mechanism. One can guess that the energy released in the peptide cleavage and filtered by peristaltic proteasome motions provides the energy for the transport. This is a motivation of the periodic force or colored noise used in [39]. Experimentally observed mechanical transformations of the proteasome in the course of time [44–46] can be the facts in favor of this hypothesis.

The next important question is the influence of the sequence-specific cleavage strength. Indeed, different proteins have different cleavage patterns. Let us simulate the degradation of casein as in [29] with constant cleavage rates and with sequence specific cleavage rates computed with Netchop algorithms. Casein has a length of $L_p = 188$ aa and the cleavage pattern as in Figure 5 right. All other parameters are the same as in the case of the three-peak length distribution (see Figure 5, left). We have rescaled the cleavage strength to have the same mean value of 0.001. To our surprise, the length distributions of the non-sequence-specific case (Figure 7 left) and sequence-specific case (Figure 7 right) are practically identical. Hence, to model the length distribution as a result of different translocation rates, it is not so important to consider the cleavage pattern of the substrate. Of course, the cleavage pattern should by no means be taken into account if the substrate is not so long or if there is a relatively small number of cleavage sites. In this case, the cleavage pattern can significantly change the length distribution. Also, if we do not consider the length distribution but rather the generation of some specific fragments, the cleavage pattern is of crucial importance even for the degradation of long proteins, e.g., see [37].

At the present stage the transport model discussed cannot be used for quantitative predictions and serves as an illustration for an optimal length transportation hypothesis. We identify two possible directions which can be taken in order to develop the proteasome model to perform quantitative predictions and take into account translocation properties. A first possibility would be to simulate a population of proteasomes, each of them modeled with the Gillespie algorithm, as in this paper. A second option would be to take into account the length-dependent protein transport correction in kinetic models of the proteasome function, as in [37, 47]. In both cases, one should implement a specific protein sequence, which certainly influences a cleavage pattern and the proteasome–protein interaction potential, and description of in- and outfluxes, taking into account the possibility of gate opening

and closing [29]. Of course, more precise models would be based on molecular dynamics simulations, but taking into account the large quantity of atoms in this system and long degradation time, up to 5 min, this seems to be impossible with current computational facilities. Also it would be very interesting to solve an inverse problem, namely to identify the translocation rates from those experiments where the substrate length is an important parameter, as e.g., in [48]. In particular, from the ratchet model of translocation rates [39] and the model presented here it follows that the temperature decrease can result in a qualitative change of the length distribution.

Acknowledgements AZ acknowledges a financial support from the VW-Stiftung, JK and AZ from the European Union through the Network of Excellence BioSim, Contract No. LSHB-CT-2004-005137. We thank PD T. Poeschel, Prof. H.G. Holzhütter, Dr F. Luciani, Dr M. Mishto, Dr S. Witt, M. Beuttler, N. Soussanova for comments and discussions.

References

1. Coux, O., Tanaka, K., Goldberg, A.L.: Structure and functions of the 20S and 26S proteasomes. Annu. Rev. Biochem. **65**, 801–847 (1996)
2. Kloetzel, P.M.: Antigen processing by the proteasome. Nat. Rev. Mol. Cell. Biol. **2**, 179–187 (2001)
3. Tamura, T., Nagy, I., Lupas, A., Lottspeich, F., Cejka, Z., Schoofs, G., Tanaka, K., De Mot, R., Baumeister, W.: The first characterization of a eubacterial proteasome: the 20S complex of Rhodococcus. Curr. Biol. **5**, 766–774 (1995)
4. Hendill, K.B.: The 19S multicatalytic 'prosome' proteinase is a constituitive enzyme in HeLa cells. Biochem. Int. **17**, 471–478 (1988)
5. Kisselev, A.F., Akopian, T.N., Goldberg, A.L.: Range of sizes of peptide products generated during degradation of different proteins by archaeal proteasomes. J. Biol. Chem. **273**, 1982–1989 (1998)
6. Hilt, W., Wolf, D.H.: Proteasomes of the yeast *S. cerevisiae*: genes, structure and functions. Mol. Biol. Rep. **21**, 3–10 (1995)
7. Ciechanover, A.: The ubiquitin-proteasome proteolytic pathway. Cell **79**, 13–21 (1994)
8. Hochstrasser, M.: Ubiquitin-dependent protein degradation. Annu. Rev. Genet. **30**, 405–439 (1996)
9. Goldberg, A.L., Cascio, P., Saric, T., Rock, K.L.: The importance of the proteasome and subsequent proteolytic steps in the generation of antigenic peptides. Mol. Immunol. **39**, 147–164 (2002)
10. Kloetzel, P.M.: Generation of major histocompatibility complex class I antigens: functional interplay between proteasomes and TPPII. Nat. Immunol. **5**, 661–669 (2004a)
11. Lankat-Buttgereit, B., Tampe, R.: The transporter associated with antigen processing: function and implications in human diseases. Physiol. Rev. **82**, 187–204 (2002)
12. Rock, K.L., Goldberg, A.L.: Degradation of cell proteins and the generation of MHC class I-presented peptides. Annu. Rev. Immunol. **17**, 739–779 (1999)
13. Shastri, N., Schwab, S.: Producing nature's gene-chips: the generation of peptides for display by MHC class I molecules. Annu. Rev. Immunol. **20**, 463–493 (2002)
14. Adams, J., Palombella, V., Elliott, P.: Proteasome inhibition: a new strategy in cancer treatment. Invest. New Drugs **18**, 109–121 (2000)
15. Dou, Q.P., Smith, D., Daniel, K., Kazi, A.: Interruption of tumor cell cycle progression through proteasome inhibition: implications for cancer therapy. Prog. Cell Cycle Res. **5**, 441–446 (2003)
16. Orlowski, R.Z.: The role of the ubiquitin-proteasome pathway in apoptosis. Cell Death Differ. **6**, 303–313 (1999)
17. Glickman, M., Ciechanover, A.: The ubiquitin-proteasome proteolytic pathway: destruction for the sake of construction. Physiol. Rev. **82**, 373–428 (2002)
18. Sakamoto, K.: Ubiquitin-dependent proteolysis: its role in human diseases and the design of therapeutic strategies. Mol. Genet. Metab. **77**, 44–56 (2002)

19. Zeng, B.Y., Medhurst, A.D., Jackson, M., Rose, S., Jenner, P.: Proteasomal activity in brain differs between species and brain regions and changes with age. Mech. Ageing Dev. **126**, 760–766 (2005)
20. Kloetzel, P.M.: The proteasome and MHC class I antigen processing. Biochem. Biophys. Acta. **1695**, 225–233 (2004b)
21. Rechsteiner, M., Realini, C., Ustrell, V.: The proteasome activator 11S REG (PA28) and class I antigen presentation. Biochem. J. **345**, 1–15 (2000)
22. Peters, J.M., Cejka, Z., Harris, J.R., Kleinschmidt, J.A., Baumeister, W.: Structural features of the 26S proteasome complex. J. Mol. Biol. **234**, 932–937 (1993)
23. Akopian, T.N., Kisselev, A.F., Goldberg, A.L.: Processive degradation of proteins and other catalytic properties of the proteasome from *Thermoplasma acidophilum*. J. Biol. Chem. **272**, 1791–1798 (1997)
24. Rapin, N., Kesmir, C., et al..: Integrating bioinformatics and systems biology for modelling of the immune system. J. Biol. Phys. (2006)
25. Cascio, P., Hilton, C., Kisselev, A.F., Rock, K.L., Goldberg, A.L.: 26S proteasomes and immunoproteasomes produce mainly N-extended versions of an antigenic peptide. EMBO J. **20**, 2357–2366 (2001)
26. Nussbaum, A.: From the test tube to the world wide web: the cleavage specificity of the proteasome. PhD thesis, Eberhard-Karls-Universitaet Tuebingen (2001)
27. Nussbaum, A.K., Dick, T.P., Kielholz, W., Schirle, M., Stevanovic, S., Dietz, K., Heinemeyer, W., Groll, M., Wolf, D.H., Huber, R., Rammensee, H.G., Schild, H.: Cleavage motifs of the yeast 20S proteasome β subunits deduced form digests of enolase 1. Proc. Natl. Acad. Sci. USA **95**, 12504–12509 (1998)
28. Wenzel, T., Eckerskorn, C., Lottspeich, F., Baumeister, W.: Existence of a molecular ruler in proteasomes suggested by analysis of degradation products. FEBS Lett. **349**, 205–209 (1994)
29. Köhler, A., Cascio, P., Leggett, D.S., Woo, K.M., Goldberg, A.L., Finley, D.: The axial channel of the proteasome core particle is gated by the Rpt2 ATPase and controls both substrate entry and product release. Mol. Cell (7), 1143–1152 (2001)
30. Kuttler, C., Nussbaum, A.K., Dick, T.P., Rammensee, H.G., Schild, H., Hadeler, K.P.: An algorithm for the prediction of proteasomal cleavages. J. Mol. Biol. **298**, 417–429 (2000)
31. Kesmir, C., Nussbaum, A., Schild, H., Detours, V., Brunak, S.: Prediction of proteasome cleavage motifs by neural networks. Protein Eng. **15**, 287–296 (2002)
32. Tenzer, S., Peters, B., Bulik, S., Schoor, O., Lemmel, C., Schatz, M.M., Kloetzel, P.M., Rammensee, H.G., Schild, H., Holzhütter, H.G.: Modeling the MHC class I pathway by combining predictions of proteasomal clavage, TAP transport and MHC class I binding. CMLS, Cell. Mol. Life Sci. **62**, 1025–1037 (2005)
33. Schmidtke, G., Emch, S., Groettrup, M., Holzhuetter, H.G.: Evidence for the existence of a non-catalytic modifier site of peptide hydrolysis by the 20S proteasome. J. Biol. Chem. **275**, 22056–22063 (2000)
34. Stein, R.L., Melandri, F., Dick, L.: Kinetic characterization of the chymotrypic activity of the 20S proteasome. Biochemistry **35**, 3899–3908 (1996)
35. Stohwasser, R., Salzmann, U., Giesebrecht, J., Kloetzel, P.M., Holzhuetter, H.G.: Kinetic evidence for facilitation of peptide channelling by the proteasome activator PA28. Eur. J. Biochem. **267**, 6221–6230 (2000)
36. Holzhütter, H.G., Kloetzel, P.M.: A kinetic model of vertebrate 20S proteasome accounting for the generation of major proteolytic fragments from oligomeric peptide substrates. Biophys. J. **79**, 1196–1205 (2000)
37. Peters, B., Janek, K., Kuckelkorn, U., Holzhütter, H.G.: Assessment of proteasomal cleavage probabilities from kinetic analysis of time-dependent product formation. J. Mol. Biol. **318**, 847–862 (2002)
38. Gillespie, D.: A general method for numerically simulating the stochastic time evolution of coupled chemical reactions. J. Comput. Phys. **22**, 403–434 (1976)
39. Zaikin, A., Pöschel, T.: Peptide-size-dependent active transport in the proteasome. Europhys. Lett. **69**, 725–731 (2005)
40. Landa, P., Zaikin, A., Schimansky-Geier, L.: Effect of the potential shape and of a Brownian particle mass on noise-induced transport. Chaos, Solitons Fractals **12**, 1459–1471 (2001)
41. Brokaw, C.: Protein–protein ratchets: stochastic simulation and application to processive enzymes. Biophys. J. **81**, 1333–1344 (2001)
42. Bier, M.: Processive motor protein as an overdamped brownian stepper. Phys. Rev. Lett. **91**, 148104 (2003)

43. Jung, P., Hänggi, P.: Resonantly driven Brownian motion: basic concepts and exact result. Phys. Rev. A **41**, 2977 (1990)
44. Gaczynska, M., Osmulski, P.A., Gao, Y., Post, M.J., Simons, M.: Proline- and Arginine-rich peptides constitute a novel class of allosteric inhibitors of proteasome activity. Biochemistry **42**, 8663–8670 (2003)
45. Osmulski, P.A., Gaczynska, M.: Atomic force microscopy reveals two conformations of the 20S. J. Biol. Chem. **275**, 13171–13174 (2000)
46. Osmulski, P.A., Gaczynska, M.: Nonoenzymology of the 20S proteasome: proteasomal actiona are controlled by the allosteric transitions. Biochemistry **41**, 7047–7053 (2002)
47. Luciani, F., Kesmir, C., Mishto, M., Or-Guil, M., de Boer, R.J.: A mathematical model of protein degradation by the proteasome. Biophys. J. **88**, 2422–2432 (2005)
48. Dolenc, I., Seemüller, E., Baumeister, W.: Decelerated degradation of short peptides by the 20S proteasome. FEBS **434**, 357–361 (1998)